Journal of Catalysis 275 (2010) 25–33

Contents lists available at ScienceDirect

Journal of Catalysis

journal homepage: www.elsevier.com/locate/jcat

Perovskite-type oxide catalysts for low temperature, anaerobic catalytic partial oxidation of methane to syngas

Federica Mudu [a], Bjørnar Arstad [b,c,*], Egil Bakken [b], Helmer Fjellvåg [a,c], Unni Olsbye [a,c,**]

[a] Centre of Material Science and Nanotechnology, Department of Chemistry, University of Oslo, P.O. Box 1126 Blindern, N-0318 Oslo, Norway
[b] SINTEF Materials and Chemistry, Forskningsveien 1, 0314 Blindern, Oslo, Norway
[c] inGAP Centre of Research-Based Innovation, Department of Chemistry, University of Oslo, P.O. Box 1126 Blindern, N-0318 Oslo, Norway

ARTICLE INFO

Article history:
Received 15 March 2010
Revised 25 June 2010
Accepted 4 July 2010
Available online 21 August 2010

Keywords:
Perovskite oxide
Synthesis gas
Methane partial oxidation
Reducible oxide
Thermogravimetric analysis
Rhodium

ABSTRACT

The cyclic reaction between CH_4 and O_2 over perovskite-type $La_{0.8}Sr_{0.2}Fe_{0.8}Co_{0.2}O_{3-\delta}$, $La_{0.75}Sr_{0.25}Fe_{0.6}Co_{0.15}Al_{0.25}O_{3-\delta}$ and $La_{0.8}Sr_{0.2}Fe_{0.8}Co_{0.2}O_{3-\delta}$/γ-AlO(OH), impregnated with 0.5 wt% Rh or Pt, was studied at 873 K. Synchrotron X-ray and neutron diffraction patterns of $La_{0.75}Sr_{0.25}Fe_{0.6}Co_{0.15}Al_{0.25}O_{3-\delta}$ proved a rhombohedral structure with Al distributed over the octahedral B-site. The oxygen non-stoichiometry (δ) was determined by thermogravimetric analysis at 958 K for $pO_2 > 10^{-22}$ atm. High selectivity to the partial oxidation products CO and H_2 was observed when $3-\delta$ was lower than 2.76 and 2.78 for the mentioned oxides, with and without Al, respectively. The role of Rh relates solely to the activation of CH_4. A stable high selectivity throughout the pulse sequence was achieved when utilizing partially reduced materials. In situ synchrotron XRD proved that the oxides retained the perovskite structure during the reduction/oxidation cycle, and no phase decomposition occurred. The strong correlation between results from catalytic transient tests and thermogravimetric analysis suggests that the CO selectivity is ruled by the redox potential of the reducible oxide.

1. Introduction

The worldwide demand for natural gas (NG) is expected to continue its long-term upwards trend in the next decades [1,2] with a slight increase in the share of unconventional gas [2]. Offshore, remote NG represents a particular exploitation challenge, since floating units for conversion of NG to easily transportable liquid products (methanol or synthetic crude oil) need to be light-weight and free of explosion risks associated with e.g. air distillation.

Conventional technologies for conversion of NG to methanol or synthetic crude proceed via synthesis gas (syngas; $CO + H_2$) production over transition-metal (Ni in particular)-based catalysts [3]. In order to obtain the appropriate H_2:CO ratio in the syngas, either steam reforming, followed by the water gas shift reaction (reactions (1) and (2), respectively) or autothermal reforming (3), may be used. The latter is a complex process comprising combustion of part of the feed (4) followed by reactions (1) and (2) [4].

$$CH_4 + H_2O \rightarrow CO + 3H_2 \quad (1)$$
$$CO + H_2O \leftrightarrow H_2 + CO_2 \quad (2)$$
$$CH_4 + 0.5O_2 \rightarrow CO + 2H_2 \quad (3)$$
$$CH_4 + 2O_2 \rightarrow CO_2 + 2H_2O \quad (4)$$

The product compositions are determined by thermodynamics. Both CH_4 conversion and CO and H_2 selectivities are favored by high temperatures and low pressures. Common outlet temperatures in industrial processes are above 1000 K [3].

For offshore purposes, a small light-weight unit for syngas production is desirable. Steam reforming units are limited by heat transfer and typically consist of 5–600 reactor tubes, each with a diameter of 70–130 mm [3], and do not meet relevant weight requirements. On the other side, autothermal reforming uses a much more compact reactor, but the process involves the use of pure O_2, commonly produced via cryogenic distillation and associated with non-zero explosion risks [5]. Such high temperature processes are furthermore demanding with respect to materials choice. For these reasons, a low-risk, low- or medium-temperature process for selective oxidation of CH_4 to syngas would represent an attractive alternative.

One possible approach would be a selective oxidation process, in which a reducible metal oxide is used as O_2 source (5) and subsequently reoxidized in an air separation unit (6).

$$yCH_4 + MO_x = yCO + 2yH_2 + MO_{x-y} \quad (5)$$
$$MO_{x-y} + 1/2yO_2 = MO_x \quad (6)$$

Such split oxidation process has been widely studied for several partial oxidation reactions [6,7], and was evaluated already in 1949 by Lewis et al. for conversion of CH_4 to syngas using CuO as oxygen source in a fluidized bed reactor at around 1200 K [8]. They

* Corresponding author.
** Corresponding author. Address: inGAP Centre of Research-Based Innovation, Department of Chemistry, University of Oslo, P.O. Box 1126 Blindern, N-0318 Oslo, Norway.
E-mail address: unni.olsbye@kjemi.uio.no (U. Olsbye).

0021-9517/$ - see front matter © 2010 Elsevier Inc. All rights reserved.
doi:10.1016/j.jcat.2010.07.004

suggested a two-step reaction; a first step where copper oxide was rapidly reduced and part of CH_4 totally oxidized, and a second slower step where the CH_4 was reformed with the formed carbon dioxide and steam to syngas.

More recently, Otsuka et al. investigated ceria, CeO_2, as oxidant in CH_4 partial oxidation to syngas [9]. Ceria is one of the best known oxygen storage materials and is e.g. used in three way catalysts [10,11]. Several recent works describe ceria as oxidizer for the conversion of CH_4 to syngas [12–16]. Ceria is often combined with platinum to increase the activity at low temperatures and/or chemically modified with e.g. zirconium, samarium or bismuth to tune oxygen diffusivity and capacity [17]. An important issue is syngas selectivity. Otsuka observed high syngas selectivities over Pt/CeO_2 and suggested that CO and H_2 were formed directly from CH_4 [9,12], but did not discuss total oxidation products. Later, Fathi et al. studied Pt and Rh supported on CeO_2 and observed that syngas selectivity depended on the degree of reduction of ceria [14]. Pantu et al. made the same observation for Pt and Ru supported on $Ce_{1-x}Zr_xO_2$ and suggested that the selectivity to CO and H_2 is determined by the relative rates of CH_4 and CO oxidation [15].

Perovskite-type oxides (ABO_3) represent an alternative class of reducible oxides with potential as partial oxidation catalysts [18]. Previously, such studies of reactions (5) and (6) have focused on high temperature applications (above 1073 K) due to low activity [19–23]. Dai et al. studied $LaFeO_3$ and suggested that full combustion products are formed from chemisorbed oxygen at particle surfaces, while selective oxidation products are formed from oxygen diffusing from the bulk [24]. Recently, Kharton et al. reported a correlation between the degree of reduction and the activity and selectivity for syngas formation over $La_{0.3}Sr_{0.7}Fe_{0.8}M_{0.2}O_{3-\delta}$ (M = Ga, Al) and $SrFe_{0.7}Al_{0.3}O_{3-\delta}$ [25].

In the present study, Rh-promoted (La, Sr)(Fe, Co, Al)$O_{3-\delta}$ perovskites were studied as CH_4 partial oxidation catalysts at medium temperatures (873 K). The purpose of the study was to elucidate the reason for the reported oxide non-stoichiometry–syngas selectivity correlation and further to elaborate the phase stability and oxygen capacity of a novel perovskite composition for the title reaction.

The materials were characterized in detail by in situ and ex situ powder X-ray diffraction (XRD), neutron diffraction, thermogravimetric methods and cyclic fixed bed reactor tests. The results provide novel insight into materials – selectivity correlation, providing a basis for future design of oxidizers for selective oxidations.

2. Experimental

2.1. Synthesis

Perovskite oxides with nominal formula $La_{0.8}Sr_{0.2}Fe_{0.8}Co_{0.2}O_{3-\delta}$ (LSFC) and $La_{0.75}Sr_{0.25}Fe_{0.6}Co_{0.15}Al_{0.25}O_{3-\delta}$ (LSFCA) were prepared by the citric acid method. $Sr(NO_3)_2$ (Fluka, ⩾99.0), Co(II)acetate tetrahydrate (Fluka, ⩾99.0), La_2O_3 (Sigma–Aldrich, 99.99), $Al(NO_3)_3{\cdot}9H_2O$ (Merck, ⩾99.0) and $Fe(NO_3)_3{\cdot}9H_2O$ (Merck, ⩾99.0) were used as reagents. La_2O_3 was dissolved in nitric acid, and the other reactants were dissolved in water before mixing. A surplus of citric acid monohydrate ($C_6H_8O_7{\cdot}H_2O$, 100%, VWR) was then added. The mixture was heated to 430 K and held at this temperature until dry. For one sample, boehmite (AlOOH Vista Chemical Company) was added to the viscous LSFC mixture before drying, resulting in a composite material (65 wt% $La_{0.75}Sr_{0.25}Fe(Co)_{0.75}Al_{0.25}O_3$, 20 wt% $LaFe(Co)Al_{11}O_{19}$ and 15 wt% $Fe(Co)Al_{12}O_4$) with cation ratio La:Sr:Fe:Co:Al = 4:1:4:1:12 (denoted LSFCB, where B stands for Boehmite). The dried gels were crushed and heated to 720 K at a rate of 5 K/min, held for 1000 min, and thereafter the temperature was raised to 1273 K (5 K/min) and held for 1000 min. The 1273 K treatment was carried out twice with crushing between each treatment. Rh was deposited using the incipient-wetness technique to a nominal amount of 0.5 wt% (elemental Rh). $Rh(NO_3)_3{\cdot}2H_2O$ from Alfa-Aesar was used. After impregnation, the Rh/LSFC, Rh/LSFCA and Rh/LSFCB samples were heated at a rate of 5 K/min to 1073 K and held for 600 min. Additional Rh/LSFCA were synthesized with 0.1 wt% and 1.0 wt% Rh loading.

2.2. Characterization

BET surfaces of the samples were estimated using single point isotherm measurements on a Quantachrome Monosorb instrument at 77 K (liquid N_2).

Powder X-ray diffraction patterns were recorded with a position sensitive detector using a Siemens Bruker D5000 diffractometer and Cu $K\alpha_1$ radiation. Room temperature Neutron Powder Diffraction (NPD) data were collected with PUS (Powder Universal Spectrometer) two-axis diffractometer at the JEEP-II reactor at Kjeller, Norway. Data were collected over a 2Θ range of 10–130° using neutrons of wavelength 1.5561 Å and rebinned into steps of 0.05°.

Variable temperature synchrotron radiation X-ray diffraction (SRXRD) patterns were collected on a MAR345 image plate system at the Swiss-Norwegian Beam Line (SNBL) at ESRF, Grenoble, France, at a wavelength of 0.694 Å. The detector resolution at the working distance used corresponds to an effective step size of 0.01783° in 2Θ. The analyzed 2Θ range was 1–40°. With an exposure time of 20 s and read out time of 87 s, the time resolution between consecutive scans is 107 s. The sample (0.1–0.2 mm diameter particles) was loaded between two quartz wool pads in a 0.7 mm diameter quartz capillary. Both ends of the capillary were mounted to a flow cell by means of Swagelok valves. The inlet was connected to a gas feed system and the outlet to a Mass Spectrometer (Pfeiffer Omnistar) for continuous effluent analysis. The gas feed system was equipped with Bronkhorst mass flow controllers and remotely controlled. An air heater gun with remote temperature control was used for heating. Temperature calibration was carried out by separate measurements of the thermal expansion of silver. During the *in situ* experiments, Rh/LSFC and Rh/LSFCB were heated to 1000 K in an O_2:He = 10:90 gas flow. Once the temperature was stable, the gas flow was switched to CH_4:He = 10:90 for 15 min, thereafter switched back to O_2 for 15 min, before a second CH_4 and O_2 sequence, and finally cooled to 800 K and subjected to two reduction–oxidation cycles.

Rietveld refinements of the NPD data and batch refinements of the SRXRD patterns were performed using the GSAS/EXPGUI [26,27] suite of programs. Peak shape was modeled using modified Gaussian (NPD) and pseudo-Voigt (XRD) profile functions.

2.3. Thermogravimetric analysis (TG)

TGA experiments were performed to investigate the equilibrium oxygen non-stoichiometry ($3-\delta$) of Rh/LSFCA and Rh/LSFC as a function of O_2 partial pressure (pO_2) at 958 K. Samples of (typically) 100 mg were measured by a SETARAM Setsys Evolution TGA with an in-house gas mixing system giving 100 ml min^{-1} reaction gas. The gas mixing system allowed successive dilution of the reaction gas to obtain a wide range of O_2 partial pressures. CO_2 and H_2 with different dilutions were used to obtain the lower pO_2 reaction gas mixtures, and pO_2 values were measured with a pO_2 sensor built in house. The non-stoichiometry versus pO_2 isotherms were measured for O_2 partial pressures in the range 10^{-22}–2×10^{-1} atm. The absolute stoichiometry ($3-\delta$) of the samples in air at room temperature was determined by cerimetric titration. The $3-\delta$ variation from room temperature to 958 K was measured thermogravimetrically, thus providing the absolute $3-\delta$ value at 958 K. XPS measurements (not reported here) showed that Rh was

oxidized after pretreatment in air at 973 K and reduced after pretreatment in 10% CH_4 at the same temperature. Therefore, the oxygen loss due to Rh_2O_3 reduction to metallic Rh was subtracted before the $3-\delta$ was calculated, in the thermogravimetric measurements, as well as in the catalytic measurements (see below).

2.4. Catalytic tests in pulse setup

Catalytic testing was performed in a tubular quartz reactor (i.d. 8 mm) at 873 K and 1 atm pressure. The catalyst (0.1 g, 0.2–0.5 mm diameter) was diluted by quartz (0.4 g, 0.2–0.5 mm). An automated setup equipped with 4-way and 6-way VICI VALCO valves was used. Feed gases (AGA, 99.996%) were used without further purification, implying an O_2 content not higher than 1×10^{-5} atm. The 4-way valve was used to switch between 10% CH_4/He and 10% O_2/He. The 6-way valve was equipped with a loop (0.25 ml) and used to send discrete pulses of gas, with a continuous stream of Ar (30 ml/min), to the reactor. In one experiment, O_2 pulses were sent to the reactor every 2 min, while the catalyst was heated to 873 K. The sample was equilibrated in Ar flow for 10 min at 873 K and thereafter subjected to a series of 50 CH_4 pulses (10% CH_4/He) followed by a series of 100 O_2 pulses (10% O_2/He). The same test was performed on Rh/LSFC and Rh/LSFCA at 958 K. However, in this case, the sample was equilibrated in Ar flow for 24 h before proceeding with CH_4 pulses.

In a second set of experiments, the cycling properties of the materials were studied. The catalyst was heated to 873 K as described above, then 50 pulses of CH_4 were let into the reactor followed by 14 pulses of O_2. Subsequently, 25 pulses of CH_4 followed by 14 pulses of O_2 were sent to the reactor. This reduction–oxidation cycle was repeated 13 times.

Effluent gases were monitored by an online mass spectrometer (Pfeiffer Omnistar). Calibration values for quantification of CH_4, CO_2, CO and H_2 were found by sending known pulses of these gases and integrating the area under the peaks of *m/z* 15, 44, 28 and 2, respectively. The contribution of CO_2 to *m/z* 28 was accounted for before quantification of CO. Carbon balance was calculated for each pulse as the sum of unconverted CH_4, CO_2 and CO. H_2O was quantified as the difference of the converted CH_4 and the produced H_2.

3. Results and discussion

3.1. Structural properties and phase analysis

Powder X-ray diffractograms (XRD) of the studied oxides are shown in Fig. 1. The observed peaks and their splitting clearly showed that LSFC and LSFCA took rhombohedral symmetry, in good accordance with the findings by Riza et al. for $La_{0.8}Sr_{0.2}Fe_{0.8}Co_{0.2}O_{3-\delta}$. However, they reported that even small compositional variations could change the symmetry to orthorhombic [28]. Earlier, Tai et al. [29] had reported orthorhombic symmetry for the mentioned stoichiometry. Unit cell dimensions for the rhombohedral LSFC sample as derived from Rietveld refinements are listed in Table 1.

Analysis of synchrotron powder X-ray diffraction data for the AlOOH-containing LSFCB revealed the presence of several crystalline phases (Fig. 2). Two aspects were of interest; minor Al-substitutions to modified redox features of the oxide, and large additions to provide an alumina-rich support for the redox-active perovskite. For the Al-rich LSFCB sample, the latter multiphase situation was expected. The perovskite-type main phase was rhombohedral (like LSFC), but with lower unit cell volume and a lower degree of distortion. The second main phase was lanthanum iron hexaaluminate ($LaFeAl_{11}O_{19}$) with smaller amounts of $FeAl_2O_4$ in addition. These Al-rich oxides originated from the boehmite added in the synthesis. $LaFeAl_{11}O_{19}$ is interesting in itself for catalytic applications [30–32]. It has a stable specific surface area even after prolonged treatments

Table 1
Surface area and refined unit cell values.

Sample	BET Surface area (m^2/g)	*a*	*c*	Space group
LSFC	1.5	5.502	13.347	R-3C
LSFCB	17.9	5.474	13.328	R-3C
LSFCA[a]	3.5	5.472	13.323	R-3C
Rh/LSFC	1.8			
Rh/LSFCB	19			
Rh/LSFCA	4.3			

[a] Refined values from NPD. La, Sr in 6a 0,0,1/4; Fe, Co in 6b 0,0,0 and O in 18e *x*,0,1/4, *x* = 0.5387 (2).

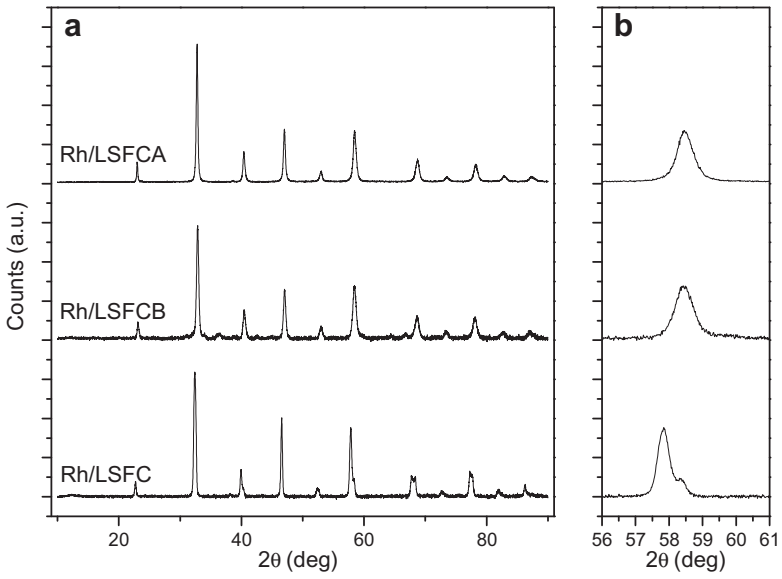

Fig. 1. (a) Powder X-ray diffraction patterns for Rh/LSFC, Rh/LSFCB and Rh/LSFCA. Inset (b) emphasizes similarity in pattern between Rh/LSFCB and Rh/LSFCA when compared to Rh/LSFC. In (b) merging of the three reflections (3 0 0), (2 1 4 and (0 1 8) centered at 58° in Rh/LSFCB and Rh/LSFCA is evident, reflecting a lower degree of rhombohedral distortion.

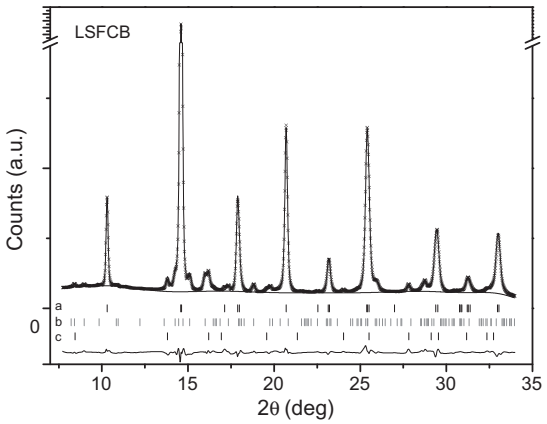

Fig. 2. Observed, calculated and difference powder diffraction pattern for LSFCB. The bars indicate reflections from the different phases present in the material, perovskite oxide (a), lanthanum iron hexaaluminate $LaFe_1Al_{11}O_{19}$ (b), and spinel $FeAl_2O_4$ (c).

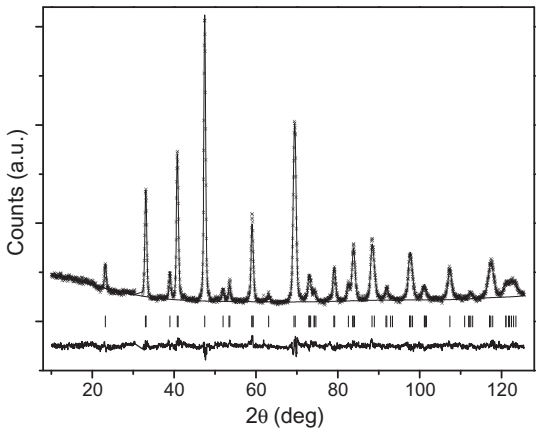

Fig. 3. Observed, calculated, and difference powder neutron diffraction pattern for LSFCA. The bars indicate positions for perovskite oxide reflections.

at high temperature [30] and can incorporate transition elements like Cr, Mn, Fe, Co and Ni. Due to this flexibility, the present $LaFeAl_{11}O_{19}$ may take a slightly deviating composition since Sr may enter the La site, while Co could take the Fe site and Fe can easily enter the Al site. Indeed, the unit cell size measured in this work was slightly bigger than the reference $LaFeAl_{11}O_{19}$ (ICSD 203003), this deviation might originate from a partial substitution of Al with Fe (see ICSD 35174). This would in turn modify the stoichiometry of the perovskite phase. This could be evidenced through unit cell changes. Such were indeed observed when comparing LSFC and LSFCB (Table 1). On the other hand, the dominating effect currently appeared to be aluminum incorporated into the B-site. According to Rietveld refinement of LSFCB (for fit see Fig. 2), some 25% of the B-site atoms were aluminum; i.e. $La_{0.75}Sr_{0.25}Fe_{0.60}Co_{0.15}Al_{0.25}O_{3-\delta}$ (note that since Fe and Co have too similar scattering factors to be distinguished by XRD analysis, their relative amount was fixed to the nominal 0.8:0.2).

With respect to the catalytic tests reported below, it should be noted that the third target material, LSFCA, was aimed to correspond completely to the pure perovskite phase identified in the LSFCB composite. This was confirmed by analysis of neutron powder diffraction data of LSFCA (Fig. 3) and the derived unit cell data in Table 1. The neutron data strongly supported the Al-concentration at the B-site as determined from SRXRD data for LSFCB. Furthermore, the strong scattering from oxygen atoms allowed a reasonable determination of the oxygen stoichiometry. The Rietveld refinement of O-occupancy factors gave close to fully occupied O-sites ($n_o = 0.99(1)$), suggesting $\delta \approx 0$ at room temperature for LSFCA as confirmed by cerimetric titration. The rhombohedral distortion of LSFCA was less than for LSFC, i.e. the rhombohedral α angle is lowered from 60.43° to 60.22°. As a consequence, the obviously split reflections for LSFC merged into a single peak for LSFCA and LSFCB in Fig. 1 (note that peak broadening owing to strain and particle size also partly blurred the splitting). This variation in distortion was in agreement with what would be predicted from tolerance t-factor correlations using ionic radii provided by Shannon [33]; i.e. $t = 0.978$ for LSFCA whereas 0.963 for LSFC.

3.2. In situ synchrotron radiation X-ray diffraction

The 0.5 wt% Rh impregnated samples of LSFC and LSFCB were analyzed with variable temperature synchrotron radiation X-ray diffraction (SRXRD). The results are reported in Fig. 4 and in supporting information, Figs. S1 and S2. The study (Fig. 4) indicates that both the Rh/LSFC and Rh/LSFCA perovskites were stable toward segregation during cyclic operation at 800 and 1000 K. As expected, expansion of the unit cell occured upon reduction, this is due to the fact that ionic radii of Fe and Co will increase upon reduction. There was a concomitant symmetry change from rhombohedral to cubic (see Fig. S3) [34]. The pseudocubic unit cell (cube root of lattice volume per ABO_3) dimensions are shown as function of temperature and gas atmosphere in Fig. 4. In most cases, the change in unit cell size and symmetry was completed within the time frame needed to record one diffractogram (107 s). The unit cell volume change during cycling between O_2 and CH_4 atmosphere was a function of chemical composition. The ~0.4% expansion during reduction for Al-containing LSFCA was just around half of that of the parent LSFC (~0.8%) material. It is not likely that this difference can be ascribed to the degree of reduction since the oxygen consumption data in Table 2 and Fig. 5 suggest that the oxygen donation capacities differ by less than 20%. We rather suggest that structural aspects are in play; Al does not readily take tetrahedral coordination in perovskite-type oxides and may possibly stabilize e.g. square pyramidal coordination in the reduced state. These provide in turn a more efficient packing than tetrahedral building units.

3.3. Thermogravimetric analysis

At equilibrium, the oxygen non-stoichiometry for the perovskite oxide depends on temperature and O_2 partial pressure.

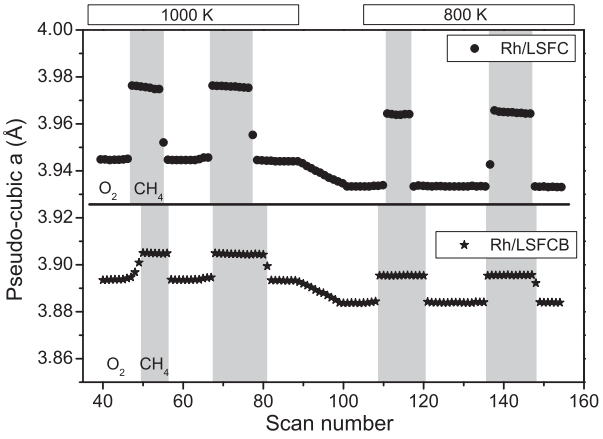

Fig. 4. Unit cell size (here reported as pseudocubic for sake of comparison) variation as a function of temperature and gas atmosphere (CH_4 intervals shown in grey) for Rh/LSFC and Rh/LSFCA. The unit cell side was determined by the Rietveld refinement of each diffractogram collected with Synchrotron X-ray diffraction.

Table 2
Pulse test results. Accumulated carbon deposition and oxygen consumption during 50 methane pulses.

Sample	CH_4 conversion (%)	CO selectivity (%)	C deposited ($\mu mol/g^{-1}$)	O used ($\mu mol/g^{-1}$)	CO_2 ($\mu mol/g^{-1}$)	CO ($\mu mol/g^{-1}$)	H_2 ($\mu mol/g^{-1}$)
LSFC	24	2	nd	46	11	<1	<1
LSFCB	16	4	nd	25	6	<1	<1
LSFCA	28	<1	nd	48	12	<1	<1
Rh/LSFC	75	43	nd	109	23	17	34
Rh/LSFCB	99	73	10	81	14	37	81
Rh/LSFCA	95	58	4	105	20	25	60
Rh/LSFCA[a]	94	85	nd	35	3	21	43

[a] Only partially reoxidized, cumulative results after 25 methane pulses.

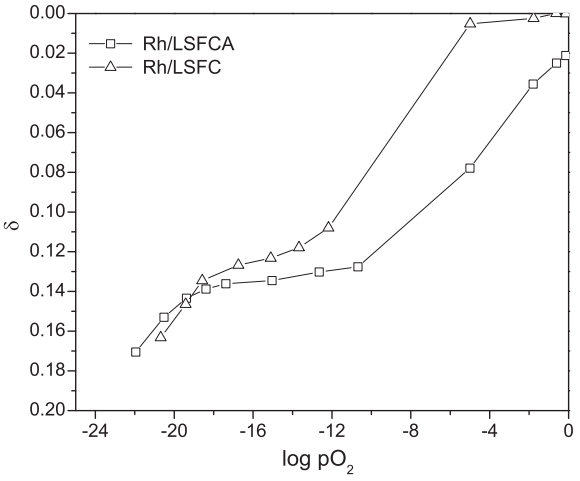

Fig. 5. Oxygen non-stoichiometry (3-δ) as a function of oxygen partial pressure as measured by thermogravimetric analysis for Rh/LSFCA and Rh/LSFC.

Thermogravimetry was used to measure the equilibrium oxygen non-stoichiometry of Rh/LSFC and Rh/LSFCA, by fixing the pO_2 of the gas mixture flowing over the oxide and keeping the temperature constant. pO_2 was varied in the range 10^{-22}–2×10^{-1} atm. Equilibrium was insured by monitoring the weight loss and allowing the samples to reach constant weight at each pO_2, in some cases this required several hours.

The equilibrium non-stoichiometry (δ) as a function of O_2 partial pressure at 958 K for Rh/LSFC and Rh/LSFCA is reported in Fig. 5. These data show the behavior of the pure perovskite oxides, i.e. the contribution from Rh_2O_3 reduction was taken into consideration (see experimental section). The oxygen stoichiometry at room temperature was measured by cerimetric titration. For both samples, a value of 3.0 was found. The initial starting $3-\delta$ value at 958 K was determined as described in Section 2.4. The initial $3-\delta$ is 3 for Rh/LSFC and 2.975 for Rh/LSFCA. This corresponds to an average valence for the B-site of 3.2 for both samples. In the case of Rh/LSFC, the $3-\delta$ was quite independent of pO_2 in the range $pO_2 > 5.0 \times 10^{-5}$ atm, while it decreased continuously in the same range for Rh/LSFCA. At $pO_2 \approx 1 \times 10^{-12}$ atm, the $3-\delta$ reached a value of 2.88 for Rh/LSFC and 2.86 for Rh/LSFCA, which corresponds to an average valence for Fe and Co of 2.93 for Rh/LSFCA and 2.96 for Rh/LSFC. Over the pO_2 range 1.0×10^{-10}–1.0×10^{-20} atm $3-\delta$ was almost independent from the pO_2. These results are in good agreement with the literature where a similar plateau was reported in the case of $La_{1-x}Sr_xFeO_{3-\delta}$ for a $3-\delta$ value corresponding to an Fe valence of 3 [35]. The two materials appeared to differ considerably at high pO_2. Rh/LSFC had a rather constant oxygen non-stoichiometry in the pO_2 range 10^0–10^{-5} atm, while Rh/LSFCA was continuously reduced in the same interval. Hence, the introduction of Al into the B-site facilitates reduction already in that pO_2 range. A similar effect of Al doping on $SrFe(Al)O_{3-\delta}$ was observed by Patrakeev et al. [36] and was related to tetrahedral Al^{3+} cations that act as traps for oxygen vacancies.

3.4. Catalytic tests; CO selectivity and cycling

The LSFC, LSFCA and LSFCB materials, with and without impregnated Rh, were tested as catalysts for CH_4 partial oxidation in a transient setup at 873 K. Results from the catalytic tests are shown in Fig. 6 and Table 2. The average carbon mass balance (C_{in}/C_{out}) for all reported tests was 1.00 ± 0.02.

CH_4 conversion versus CH_4 pulse number is plotted in Fig. 6a. Rh/LSFCB showed the highest initial activity; close to 100%, while Rh/LSFCA and Rh/LSFC had 81% and 64% initial conversion, respectively. For the non-promoted catalysts, LSFCA gave the highest initial conversion; 70%, while LSFCB and LSFC showed 55% and 41%, respectively. Blank tests of CH_4:O_2 = 1:1 mixtures in an empty reactor gave less than 5% CH_4 conversion at the same temperature and feed rate.

It is well established that metal elements facilitate CH_4 activation [5]. Notably, the LSFC-based perovskite oxides were themselves active for CH_4 oxidation at the studied temperature of 873 K, even in the absence of a metal promoter. For the Rh-containing oxides, the CH_4 conversion increased during the first CH_4 pulses. This reflects probably a progressing Rh reduction in correspondence with the literature data for Rh/Al_2O_3 catalysts [37]. Subsequently, the activity decreased. For the pure oxide catalysts, the activity decreased already from the first pulse and onwards.

The CO selectivity (and H_2, cfr Fig. 7) was initially close to zero (Fig. 6b) over all materials, but increased with time on stream. For the Rh-catalysts, the CO selectivity approached 100% after about 30 pulses. Fewer pulses were required for Rh/LSFCB to reach high selectivity than for Rh/LSFCA and Rh/LSFC. The selectivity increase was concomitant with a decrease in CH_4 conversion. For the pure oxide catalysts, only LSFCB showed increasing CO selectivity with increasing pulse number, approaching 24% after 50 pulses.

Average CH_4 conversion and H_2 and CO selectivity, and accumulated carbon deposition and O_2 consumption during 50 CH_4 pulses, are listed in Table 2. It is interesting to note that carbon deposition (as monitored by CO_x evolution during subsequent O_2 pulses) was observed for Rh/LSFCA and Rh/LSFCB, i.e. the materials that gave the highest CH_4 conversion and H_2 and CO selectivities. For these two materials, the carbon balance gradually increased during the last 20 CH_4 pulses, summing up to 12% selectivity to carbon deposition during these pulses over Rh/LSFCA. It is worth noting that the LSFC sample with Al on the B-site showed higher CO yields throughout the CH_4 pulses compared to the parent material (Fig. 6 and Table 2).

Earlier studies indicated a correlation between the CO selectivity and the degree of reduction for ceria-based materials [14,15]. In order to elucidate whether such a correlation would exist for the studied reducible Rh-promoted perovskites, the CO and H_2 selectivity was plotted as a function of oxygen consumption during 50

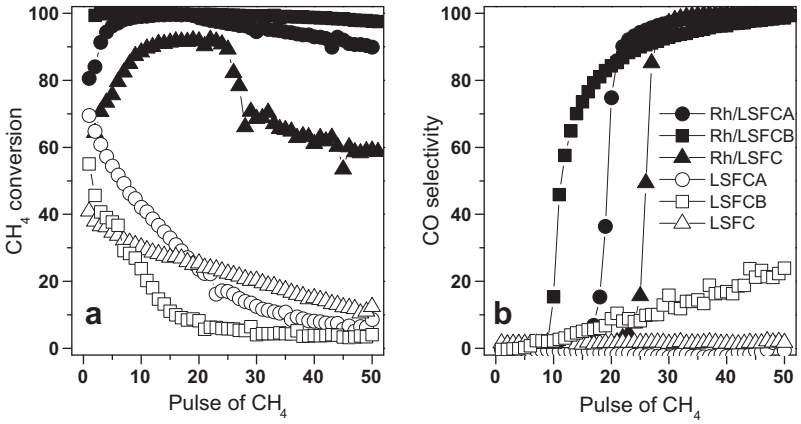

Fig. 6. Methane conversion (a) and CO selectivity (b) as function of number of methane pulses in transient catalytic tests.

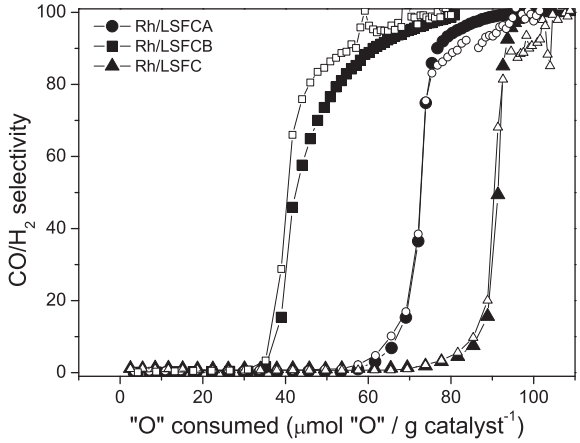

Fig. 7. CO selectivity (full symbols) and H_2 selectivity (empty symbols) as a function of consumed oxygen as registered during transient catalytic tests for Rh/LSFCA, Rh/LSFCB and Rh/LSFC.

CH_4 pulses in Fig. 7. The oxygen consumption was calculated on the basis of oxygen present in the products (CO, CO_2 and H_2O) after each CH_4 pulse. The data show clearly that the first oxygen delivered by the solid oxygen source yielded total oxidation products, whereas the subsequent oxygen release gradually led to increasing CO (and H_2) selectivity. The critical oxygen consumption ("threshold value") at which a switch in product selectivity was observed differs between the investigated materials. For the non-promoted materials, the oxygen consumption during the 50 CH_4 pulses were below the threshold values registered for the corresponding promoted materials (Fig. 7 and Table 2). This empirically explains the low CO and H_2 selectivity.

The CO and H_2 selectivity of the Rh/LSFCB was higher at lower O consumed per g of catalyst, compared to Rh/LSFCA. The reasons for this observation was the lower fraction of the perovskite oxide phase present per gram of the catalysts for LSFCB (65 wt%).

Fig. 7 suggests that a high CO and H_2 selectivity was achieved below a certain oxygen content of the reducible perovskite. If ruled solely by this parameter, one would expect that a high CO and H_2 selectivity should remain also subsequent to partial re-oxidization as long as the oxygen content remains within the selective range (i.e. below threshold). This was in turn verified by re-oxidizing Rh/LSFCA with 14 O_2 pulses (14 μmoles O_2, which corresponds approximately to the amount of CO formed during the preceding 50 CH_4 pulses, see Table 2, line 7) at 873 K. Thereafter, the catalyst was subjected to 25 CH_4 pulses followed by another 14 O_2 pulses. This group of sequences was repeated 13 times after the initial (50 + 14) pulse sequence. The first point in Fig. 8 has a low average selectivity and represents the data shown in Figs. 6 and 7. The second group of CH_4 pulse sequences gave a very high average CO selectivity (98%). Thereafter, a drop in selectivity was observed before stabilizing around the fourth group of sequences to a stable CO selectivity of 85%. The high CO selectivity obtained during the second CH_4 pulse sequence clearly supports the hypothesis that selective CH_4 partial oxidation to synthesis gas can be achieved over a partially oxidized catalyst. The decrease in average CO selectivity during the third and fourth CH_4 pulse sequences and the lower value observed during the rest of the experiment, compared to the second sequence, were due to an imbalance between the consumed and supplied oxygen.

3.4.1. Rhodium loading

The role of Rh loading was investigated for LSFCA impregnated with 0.1, 0.5 and 1 wt% Rh. The results from catalytic pulse experiments are summarized in Fig. 9 and Table 3. Fig. 9a shows the CH_4 conversion versus the number of CH_4 pulses. A significantly lower conversion for each CH_4 pulse, starting at 56%, was observed for the catalyst with the lowest Rh loading. During the first 6 CH_4 pulses, a decrease in conversion was observed followed by a plateau with

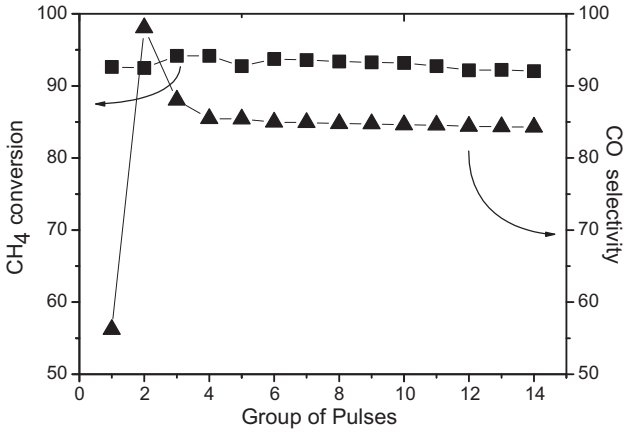

Fig. 8. CH_4 conversion and CO selectivity as a function of number of groups of pulses. Each group from nb 2–14 includes 25 methane pulses followed by 14 oxygen pulses. The first group includes 50 methane pulses followed by 14 oxygen pulses.

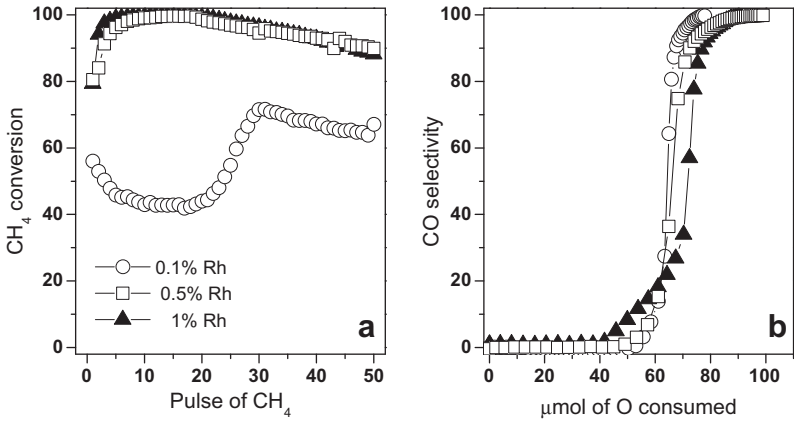

Fig. 9. LSFCA loaded with 0.1, 0.5 and 1% Rh. Methane conversion as a function of methane pulses (a) and CO selectivity as a function of consumed oxygen from the perovskite (b).

Table 3
Pulse test results for different Rh loading on LSFCA.

Rh (wt%)	CH_4 conversion	CO selectivity (%)	C deposited	O used[a]	CO_2	CO	H_2
0.1	57	41	nd	78(77)	17	12	24
0.5	94	58	4	105(99)	20	25	60
1	96	52	8	109(97)	21	23	62

[a] Numbers in brackets do not take into account the oxygen used to the Rh_2O_3 reduction.

approximately. 43% CH_4 conversion. A much higher conversion, with just a small and smooth reduction after some 20 pulses, was observed for the catalysts with 0.5 and 1.0 wt% Rh loadings.

CO selectivity versus oxygen consumption is shown for the three catalysts in Fig. 9b. The three catalysts reached 100% CO selectivity at similar oxygen consumption values. As shown in Table 3, the amount of coke on the catalyst surface after reaction increased with increasing Rh loading.

A key objective in the previous literature reports has been to develop a selective catalyst for CO and H_2 formation, according to a sequential reaction scheme [38,39]:

$$CH_4 \xrightarrow[k_a]{\text{“O”}} CO, H_2 \xrightarrow[k_b]{\text{“O”}} CO_2, H_2O \qquad (7)$$

However, there is mounting evidence that the second reaction is reversible, and rapid compared to first step for a large range of supported metal catalysts [40,41].

Reducible metal oxides, such as perovskites and ceria-based materials, may possibly contribute to a selective direct reaction pathway for partial CH_4 oxidation to synthesis gas [15,20,25]. It has been suggested that there exist two types of oxygen species in reducible oxides: one very reactive giving full oxidation and another less reactive giving predominantly partial oxidation [24,42,43]. The two oxygen species could either be ascribed to framework (“lattice”) versus loosely bound surface oxygen, or to two types of framework oxygen. Presently, the amount of surface oxygen (estimated by monolayer coverage; for specific surface area as reported in Table 1) was initially some 5 μmoles per 100 mg material. This amount was just a fraction of the oxygen consumed before reaching the threshold value and shift in selectivity toward CO, occurring around 35–70 μmoles of oxygen (Figs. 7, 9 and 10). This strongly suggests that loosely bound oxygen at the catalyst surface had no major influence on the selectivity at high pulse numbers. Thus, the framework oxygen appears to play a key role. This is supported by the experiment reported in Fig. 8, where it was shown that as long as the total oxygen content is kept below the “threshold value,” high selectivities to CO were retained during the full CH_4 pulse cycle. The observed CO selectivity does hence correlate with the degree of reduction of the perovskite oxide (Fig. 7). Notably, neither the nature nor the amount of noble metal at the surface influenced the CO selectivity (Fig. 9 and Fig. S5).

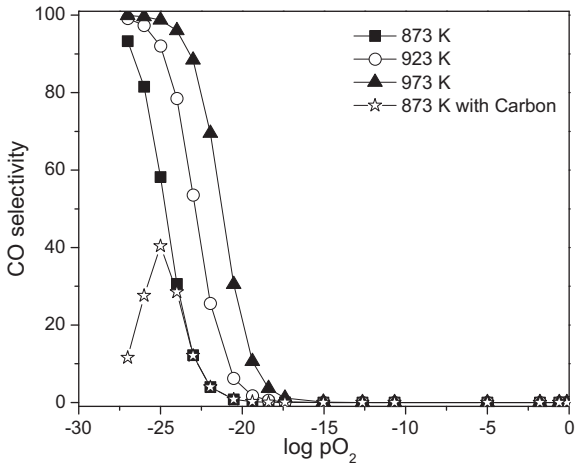

Fig. 10. Calculated CO selectivity as function of oxygen partial pressure assuming equilibrium between CO, CO_2 and O_2 (and C in one case) based on standard ΔG of formation reported in the NIST database. In the case of C, the standard ΔG reported for amorphous carbon was used.

The oxygen non-stoichiometry of the (perovskite) oxide depends at equilibrium on temperature and O_2 partial pressure [44]. At equilibrium, the partial pressure of O_2 over the oxide is directly related to its degree of reduction. This suggests that syngas selectivity over some reducible oxides might be controlled by thermodynamics just as observed in conventional catalytic partial oxidation (see below). Calculated equilibrium selectivities to CO and CO_2 versus O_2 partial pressure (at a constant carbon amount) at 873–973 K are shown in Fig. 10. CO selectivities above 90% are

predicted at O_2 partial pressure below 10^{-22} at 973 K and below 10^{-26} atm at 873 K. When including the reaction of carbon formation from CO in the calculations (considering equilibrium in both the reactions $1/2O_2 + C_a = CO$, $\Delta G_{873} = -50.42$ kJ/mol and $1/2O_2 + CO = CO_2$, $\Delta G_{873} = -49.36$ kJ/mol), using thermodynamic values for amorphous carbon at 873 K, carbon formation becomes favored over CO formation at O_2 partial pressures below 10^{-24} atm with maximum CO selectivity 40%. It should be noted that carbon formed by CH_4 decomposition may differ significantly from the amorphous carbon reported in thermodynamic tables. E.g. Rostrup-Nielsen recently reported that for noble metal-based catalysts coke-free operation of CH_4 reforming is achieved inside the C:H:O regime predicted to give amorphous carbon [45]. In the current study, carbon deposition was observed only during the 20 last pulses of a CH_4 pulse sequence (see comments to Fig. 6 and Table 2 above). We therefore assume that carbon formation was insignificant during the first 30 CH_4 pulses.

Fig. 5 shows the relation between equilibrium O_2 partial pressure over LSFC and LSFCA perovskites versus degrees of reduction, obtained by thermogravimetry. These O_2 partial pressure relations and the thermodynamic data in Fig. 10 were next used to calculate equilibrium CO selectivity versus degree of reduction of the oxide catalysts. A direct comparison between thus predicted CO selectivities (based on TG data) and measured CO selectivities (from catalytic tests) versus oxygen non-stoichiometry δ for Rh/LSFC and Rh/LSFCA is shown in Fig. 11a and b. The initial oxygen content $3 - \delta$ for the materials in the catalytic tests was set to the equilibrium value at $pO_2 = 10^{-5}$ atm, i.e. the highest pO_2 of the carrier gas. Fig. 11 shows a strong correlation between the data deduced from thermodynamic studies and from transient catalytic tests. This strongly suggests that the selectivity of the catalytic partial oxidation of CH_4 is determined by the very redox properties of the perovskites and hence by thermodynamics. The observation that the oxygen consumption before reaching high selectivity differs among the oxides (Figs. 7 and 11) is explained by the lower oxygen content in Rh/LSFCA at the start of the catalytic test (10^{-5} atm pO_2).

The present study suggests that an optimal, redox-active carrier material for anaerobic, catalytic partial oxidation of CH_4 to synthesis gas should contain a large reservoir of oxygen which is only released at low O_2 partial pressures, in the thermodynamic window between selective CO and C formation for the temperature of interest. For 0.5 wt% Rh/LSFCA at 958 K, this window is between $3 - \delta = 2.71$ and 2.78.

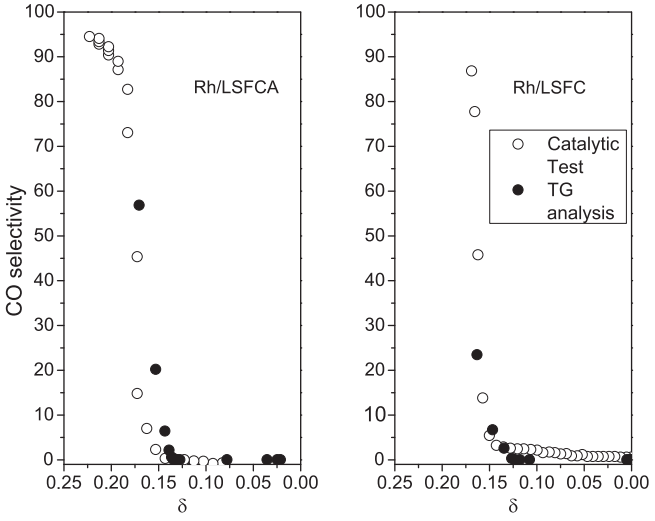

Fig. 11. CO selectivity as a function of oxygen non-stoichiometry as measured by thermogravimetric analysis and as measured by transient catalytic tests for Rh/LSFCA and Rh/LSFC.

4. Conclusion

Catalytic tests and thermogravimetric analysis have been combined to investigate the thermodynamic dependency of the CO selectivity over $La_{0.8}Sr_{0.2}Fe_{0.8}Co_{0.2}O_{3-\delta}$ and $La_{0.75}Sr_{0.25}Fe_{0.6}Co_{0.15}Al_{0.25}O_{3-\delta}$ impregnated with Rh during cyclic anaerobic CH_4 partial oxidation at 873 K. High CO yields and selectivity were obtained in an O_2 activity range below 10^{-22} atm. The perovskite-type oxygen reservoir remained stable throughout several reduction/oxidation cycles as seen by synchrotron in situ X-ray diffraction analysis. The role of Rh related solely to the activation of CH_4, without influence on selectivity. Chemical modification via Al-substitution affected the redox properties of the material and reduced the unit cell volume expansion during reduction (and cycling).

Acknowledgments

This publication is part of the Remote Gas project (168223/S30), performed under the strategic program Petromaks of The Research Council of Norway. The authors acknowledge the additional partners; Statoil, UOP, Bayerngas Norge, Aker Solutions, DNV for support.

Appendix A. Supplementary material

Supplementary data associated with this article can be found, in the online version, at doi:10.1016/j.jcat.2010.07.004.

References

[1] BP, Statistical review of world energy. <http://www.bp.com/productlanding.do?categoryId=6929&contentId=7044622>.
[2] I.E. Agency, World energy outlook fact sheet. <http://www.worldenergyoutlook.org/>.
[3] J.M. Moulijn, M. Makkee, A. Van Diepen, Chemical Process Technology, Wiley, 2001.
[4] B.C. Enger, R. Lodeng, A. Holmen, Appl. Catal. A: Gen. 346 (2008) 1–27.
[5] J.-R. Rostrup-Nielsen, in: G. Ertl, H. Knözinger, F. Schüth, J. Weitkamp (Eds.), Handbook of Heterogeneous Catalysis, Wiley, 2008, pp. 2882–2904.
[6] C.O. Bennett, in: W. Haag, B. Gates, H. Knoezinger (Eds.), Advances in Catalysis, Vol. 44, Academic Press, 2000.
[7] P. Silveston, R.R. Hudgins, A. Renken, Catal. Today, 1995, pp. 91–112.
[8] W.K. Lewis, E.R. Gilliland, W.A. Reed, Ind. Eng. Chem. 41 (1949) 1227–1237.
[9] K. Otsuka, T. Ushiyama, I. Yamanaka, Chem. Lett. (1993) 1517–1520.
[10] M. Funabiki, T. Yamada, K. Kayano, Catal. Today 10 (1991) 33–43.
[11] S. Kacimi, J. Barbier, R. Taha, D. Duprez, Catal. Lett. 22 (1993) 343–350.
[12] K. Otsuka, Y. Wang, E. Sunada, I. Yamanaka, J. Catal. 175 (1998) 152–160.
[13] K. Otsuka, Y. Wang, M. Nakamura, Appl. Catal. A: Gen. 183 (1999) 317–324.
[14] M. Fathi, E. Bjorgum, T. Viig, O.A. Rokstad, Catal. Today 63 (2000) 489–497.
[15] P. Pantu, K. Kim, G.R. Gavalas, Appl. Catal. A: Gen. 193 (2000) 203–214.
[16] V.A. Sadykov, T.G. Kuznetsova, G.M. Alikina, Y.V. Frolova, A.I. Lukashevich, Y.V. Potapova, V.S. Muzykantov, V.A. Rogov, V.V. Kriventsov, D.I. Kochubei, E.M. Moroz, D.I. Zyuzin, V.I. Zaikovskii, V.N. Kolomiichuk, E.A. Paukshtis, E.B. Burgina, V.V. Zyryanov, N.F. Uvarov, S. Neophytides, E. Kemnitz, Catal. Today 93–95 (2004) 45–53.
[17] V.A. Sadykov, T.G. Kuznetsova, Y.V. Frolova-Borchert, G.M. Alikina, A.I. Lukashevich, V.A. Rogov, V.S. Muzykantov, L.G. Pinaeva, E.M. Sadovskaya, Y.A. Ivanova, E.A. Paukshtis, N.V. Mezentseva, L.C. Batuev, V.N. Parmon, S. Neophytides, E. Kemnitz, K. Scheurell, C. Mirodatos, A.C. van Veen, Catal. Today 117 (2006) 475–483.
[18] T.V. Choudhary, S. Banerjee, V.R. Choudhary, Appl. Catal. A: Gen. 234 (2002) 1–23.
[19] Y. Zeng, S. Tamhankar, N. Ramprasad, F. Fitch, D. Acharya, R. Wolf, Chem. Eng. Sci. 58 (2003) 577–582.
[20] X.P. Dai, Q. Wu, R.J. Li, C.C. Yu, Z.P. Hao, J. Phys. Chem. B 110 (2006) 25856–25862.
[21] X. Dai, C. Yu, R. Li, Q. Wu, Z. Hao, J. Rare Earths 26 (2008) 76–80.
[22] X. Dai, C. Yu, Q. Wu, J. Nat. Gas Chem. 17 (2008) 415–418.
[23] J.N. Kuhn, U.S. Ozkan, Catal. Lett. 121 (2008) 179–188.
[24] X.P. Dai, R.J. Li, C.C. Yu, Z.P. Hao, J. Phys. Chem. B 110 (2006) 22525–22531.
[25] V.V. Kharton, M.V. Patrakeev, J.C. Waerenborgh, V.A. Sobyanin, S.A. Veniaminov, A.A. Yaremchenko, P. Gaczynski, V.D. Belyaev, G.L. Semin, J.R. Frade, Solid State Sci. 7 (2005) 1344–1352.

[26] B.H. Toby, J. Appl. Crystallogr. 34 (2001) 210–213.
[27] A.C. Larson, R.B. Von Creele, Los Alamos National Laboratory Report LAUR, 2000, pp. 86–748.
[28] F. Riza, C. Ftikos, F. Tietz, W. Fischer, J. Eur. Ceram. Soc. 21 (2001) 1769–1773.
[29] L.W. Tai, M.M. Nasrallah, H.U. Anderson, D.M. Sparlin, S.R. Sehlin, Solid State Ionics 76 (1995) 259–271.
[30] M. Machida, K. Eguchi, H. Arai, J. Catal. 103 (1987) 385–393.
[31] M. Machida, K. Eguchi, H. Arai, J. Catal. 120 (1989) 377–386.
[32] M. Machida, K. Eguchi, H. Arai, J. Catal. 123 (1990) 477–485.
[33] R.D. Shannon, Acta Crystallogr. Sect. A 32 (1976) 751–767.
[34] J.E. Readman, A. Olafsen, Y. Larring, R. Blom, J. Mater. Chem. 15 (2005) 1931–1937.
[35] J. Mizusaki, M. Yoshihiro, S. Yamauchi, K. Fueki, J. Solid State Chem. 58 (1985) 257–266.
[36] M.V. Patrakeev, V.V. Kharton, Y.A. Bakhteeva, A.L. Shaula, I.A. Leonidov, V.L. Kozhevnikov, E.N. Naumovich, A.A. Yaremchenko, F.M.B. Marques, Solid State Sci. 8 (2006) 476–487.
[37] J.C. Slaa, R.J. Berger, G.B. Marin, Catal. Lett. 43 (1997) 63–70.
[38] D.A. Hickman, L.D. Schmidt, Science 259 (1993) 343–346.
[39] Y. Boucouvalas, Z. Zhang, X. Verykios, Catal. Lett. 40 (1996) 189–195.
[40] J. Wei, E. Iglesia, J. Phys. Chem. B 108 (2004) 7253–7262.
[41] J. Wei, E. Iglesia, J. Phys. Chem. B 108 (2004) 4094–4103.
[42] R. Li, C. Yu, S. Shen, J. Nat. Gas Chem. 11 (2002) 137–144.
[43] R. Li, C. Yu, G. Zhu, S. Shen, Petrol. Sci. 2 (2005) 19–23.
[44] S. Stolen, E. Bakken, C.E. Mohn, Phys. Chem. Chem. Phys. 8 (2006) 429–447.
[45] J.R. Rostrup-Nielsen, J. Sehested, J.K. Norskov, Adv. Catal. 47 (2002) 65–139.